Proceedings of IMECE 2004
ASME International Mechanical Engineering Congress
November 13-19, 2004, Anaheim, California, USA

IMECE2004-60133

Simulation of Mist Transport for Gas Turbine Inlet Air Cooling

Ting Wang, Xianchang Li, and Venu Pinninti
Energy Conversion & Conservation Center
University of New Orleans
New Orleans, LA 70148-2220

Abstract

The output and efficiency of gas turbines are reduced significantly during the summer. Gas turbine inlet air-cooling is considered a simple and effective method to increase the power output as well as thermal efficiency. Among various cooling schemes, fog cooling (a direct evaporative cooling) has gained increasing popularity due to its simplicity and low installation cost. During fog cooling, water is atomized to micro-scaled droplets (or mist) and introduced into the inlet airflow. The inlet air temperature is reduced through water evaporation. To investigate the mist transport in the entrance duct, numerical study is performed in this paper. Different fundamental geometries are considered first, which include a straight tunnel, a diffuser, a contraction, and a 90^o bend. These geometries are used to investigate the effect of acceleration, deceleration, and centrifugal force on mist transport and cooling effectiveness, respectively. Lastly, a duct representing a real application is used. The effects of droplet size, droplet distribution, and humidity on cooled air temperature distribution are examined. Analysis on droplet history (trajectory and size) is employed to interpret the mechanism of droplet dynamics under influence of acceleration, diffusion, and body forces.

Keywords: inlet cooling, heat transfer, droplet evaporation

Nomenclature

a	thermal diffusion coefficient (m^2/s)
C	concentration (kg/m^3)
d	diameter (m)
d_{10}	arithmetic mean diameter (m)
d_{20}	surface mean diameter (m)
d_{30}	volume mean diameter (m)
d_{32}	Sauter mean diameter (m)
D	mass diffusion coefficient (m^2/s)
Dv90	90% cumulative volume frequency (m)
F	force (N)
k	turbulence kinetic energy (m^2/s^2)
k_c	mass transfer coefficient (m/s)
h	convective heat transfer coefficient (W/m^2-K)
h_{fg}	latent heat (J/kg)
L	length (m)
m	mass (kg)
Nu	Nusselt number (hd/λ)
P	pressure (N/m^2)
Pr	Prandtl number (ν/a)
Re	Reynolds number (ud/ν)
S	source term
Sc	Schmidt number (ν/D)
Sh	Sherwood number ($k_c d/D$)
T	temperature (K, ^{o}F)
t	time (s)
u	velocity component (m/s)
v	velocity component (m/s)
W	width (m)
x, y, z	coordinates

Greek

ε	turbulence dissipation (m^2/s^3)
η	cooling effectiveness $((T_{amb}-T_{exit})/(T_{amb}-T_{WBT}))$
λ	heat conductivity (W/m-K)
μ	dynamic viscosity (kg/m-s)
ν	kinematic viscosity (m^2/s)
ρ	density ($kg/m^{3)}$
τ	stress tensor ($kg/m\text{-}s^2$)

Subscript

g	gas or air
p	particle or droplet
s	surface

Introduction

High demands for electricity by most utility facilities during the hot days of summer make it essential for power plants to generate maximum output. Gas turbines are often used to meet these peek demands because of their low installation cost and short installation time. However, power output and efficiency of gas turbines reduce significantly during the summer because the air becomes less dense (which results in less mass flow rate), and the compressor's work

increases with increased ambient temperature. Every 1-^{o}F raise of ambient air temperature reduces the gas turbine output by approximately 0.3 to 0.5% [1]. To increase the power output as well as thermal efficiency, gas turbine inlet air-cooling is considered the most convenient and effective method.

In general, three different approaches can be used in gas turbine inlet air-cooling [1]. The first option is a refrigeration cooling system, either a mechanical refrigeration system or an absorption cooling system. While the mechanical refrigeration can reduce the gas turbine inlet temperature below the wet bulb temperature, the absorption system is relatively simple and has lower operation and maintenance cost than the mechanical refrigeration, and it can cool the inlet air to 50^{o}F. The second option is a thermal energy storage system that utilizes energy at off-peak hours to fill up a cold reservoir of chilled water or ice. The cold reservoir is used to cool the inlet air during peak hours. The third option is direct evaporative cooling where water evaporates directly into the airflow, and thus the air temperature reduces with a limit of the wet bulb temperature.

Among various cooling schemes, fog cooling (a direct evaporative cooling) has gained increased popularity due to its simplicity and low installation cost. More than 700 gas turbines have been installed with fog cooling [2]. During fog cooling, demineralized water is atomized to micro-scaled droplets (or mist) and introduced to the inlet airflow. The inlet air temperature is reduced through water evaporation. To improve the efficiency of the fog cooling process and its safety, many issues related to fog cooling need to be alleviated, such as run-down water on the wall, which holds the potential for water fragments to be entrained from water puddles on the floor to the compressor, and the effect of droplet dynamics on cooling uniformity in the gas turbine entrance duct. The following is a brief summary of relative studies.

Bhargava and Meher-Homji [3] presented the results of a comprehensive parametric analysis on the effect of inlet fogging on a wide range of existing gas turbines. Both evaporative and overspray fogging conditions were analyzed. It shows that the performance parameters indicative of inlet fogging effects have definitive correlation with the key gas turbine design parameters. In addition, they indicated that aero-derivative gas turbines, in comparison to the industrial machines, have higher performance improvement due to the inlet fogging effects.

Chaker et al. [2, 4-5] presented the results of extensive experimental and theoretical studies conducted over several years and coupled with practical aspects learned in the implementation of nearly 500 inlet fogging systems on gas turbines ranging from 5 to 250 MW. Their studies covered the underlying theory of droplet thermodynamics and heat transfer and provided practical points relating to the implementation and application of inlet fogging to gas turbine engines. They also described the different measurement techniques available to design nozzles. Experimental data on different nozzles and recommendations for a standardized nozzle testing method for gas turbine inlet air fogging were given. The complex behavior of fog droplets in the inlet duct was addressed and experimental results from several wind tunnel studies were documented.

Gajjar et al. [6] reported another practical example of fogging inlet cooling, which described the design, installation, commissioning, and operation of a fogging system for a large 655 MW combined cycle power plant. They discussed the special considerations as to how the fogging system could help in augmenting power during high temperature and low frequency operation of the gas turbine. Fogging helped the station maintain maximum output during the peak demand months of summer. Subsequently, the system has remained in use for short periods due to low electrical demand and part load operation of the power station. The station availability increased by approximately 2% over the year.

To validate the evaporating effect and qualify the performance of inlet cooling, Willems and Ritland [7] found that resistance temperature detectors (RTD), installed in standard thermo-wells at the inlet manifold, read wet bulb temperature long before it is actually reached. Since the accuracy of compressor inlet temperature is critical to the gas turbine operation, a modified RTD device was configured, which can shield the free moisture from air.

Mahapatra and Gilstrap [8] mentioned that it is hard to brand one atomizing method superior to another, due to lack of information about the mechanisms of atomization and droplet formation. Also the measurement of droplet size depends on the measuring location as well as the airflow properties. There is no standard widely adapted to qualify fogging systems. In another study Mahapatra and Gilstrap [9] applied psychometric principles in conducting a detailed analysis of various cooling and humidification processes accomplished by fogging systems. It was pointed out that the saturation process in an actual fog cooling system is not adiabatic. Monitoring water inlet temperature and thermodynamic parameters of airflow downstream the fogging system is important.

Most of the previous fog cooling literatures focused on design, control, and operation experiences. Limited work is given to investigate the mist transport behavior. The objective of this paper is to use CFD simulation to investigate: (a) The mechanism of droplet dynamics under influence of acceleration, diffusion, and body forces and (b) The effect of droplet size, droplet distribution, and humidity on cooling distribution and cooling effectiveness.

In this study, ducts of different simple geometries are considered first, including a straight tunnel, a diffuser, a contraction, and a 90^{o} bend, to investigate the isolated effect of acceleration, deceleration, and centrifugal force on mist transport, respectively. Then, a duct representing a real gas turbine application is applied. Analysis on droplet history (trajectory and size) is employed to interpret the mechanism of droplet dynamics.

Numerical simulations with appropriate and correct models are helpful in optimizing the nozzle locations and arrangements as well as in predicting cooling uniformity and free water particles in the entrance of the compressor (i.e. at the end of the duct).

Numerical Model

In a real application, the air/fog mixture can encounter different geometries of flow channels. For example, the air/fog mixture can pass a straight duct or a nozzle. It can also flow through a diffuser, a bend, or more complicated configurations. To study the isolated influence of acceleration, deceleration, and centrifugal force, four simple, fundamental geometries are used in this study as shown in Fig. 1. These four geometries are assigned to have the same inlet area (2×2 m^2) and the length (L) is either 8m or 10m except the bend. Although the computational domain can be one quarter of the physical geometry due to symmetry, the entire physical domain is used in computation because it is convenient to examine the trajectory of droplets, which, subject to the influence of random turbulence influence, could cross the physical symmetric planes.

The commercial software package Fluent (version 6.1.22) from Fluent, Inc. is used in this study. The simulation uses the segregated solver, which employs an implicit pressure-correction scheme. The SIMPLE algorithm is used to couple the pressure and velocity. First order upwind scheme is used to spatial discretization of the convective terms. The diffusion term is central-differenced with second-order accuracy. The Lagrangian trajectory calculations were employed to model the dispersed phase of particles, droplets, or

bubbles, including coupling with the continuous phase. The impact of the droplets on the continuous phase is considered as source terms to the governing equations. After obtaining an approximate flow field of the continuous phase (airflow in this study), Fluent traces the droplet trajectories and computes heat and mass transfer to/from them. Detailed numerical models are given next.

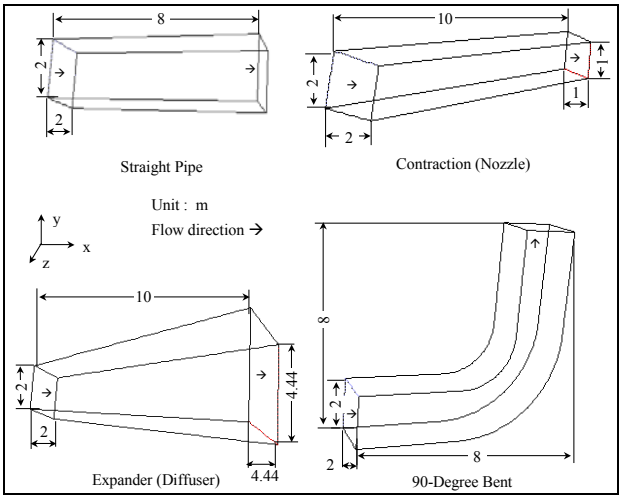

Figure 1 Four Simple Computational Geometries

Continuous Phase (Air)

Governing Equations - Considering a steady-state flow, the equations for conservation of mass, momentum, and energy can be given as:

$$\frac{\partial}{\partial x_i}(\rho u_i) = S_m \tag{1}$$

$$\frac{\partial}{\partial x_i}(\rho u_i u_j) = \rho \vec{g}_j - \frac{\partial P}{\partial x_j} + \frac{\partial \tau_{ij}}{\partial x_i} + F_j \tag{2}$$

$$\frac{\partial}{\partial x_i}(\rho c_p u_i T) = \frac{\partial}{\partial x_i}\left(\lambda_{eff}\frac{\partial T}{\partial x_i}\right) + \mu\Phi + S_h \tag{3}$$

where the source terms (S_m, F_j and S_h) are used to include the contributions from the dispersed phase. τ_{ij} is the symmetric stress tensor, which can be expressed as

$$\tau_{ij} = \mu\left(\frac{\partial u_j}{\partial x_i} + \frac{\partial u_i}{\partial x_j} - \frac{2}{3}\delta_{ij}\frac{\partial u_k}{\partial x_k}\right). \tag{4}$$

$\mu\Phi$ is the heat of dissipation and λ_{eff} is the effective heat conductivity. When turbulence effect is considered, both τ_{ij} and λ_{eff} need to be modeled.

Turbulence Modeling - The standard k-ε model is selected because the flow in this study does not involve any strong streamline curvature, vortices or rotation. The standard k-ε model is the simplest two-equation model and it is proven to be robust, economic for computation, and reasonably accurate for a wide range of turbulent flows. The equations for the turbulent kinetic energy (k) and its dissipation rate (ε) are:

$$\frac{\partial}{\partial x_i}(\rho u_i k) = \frac{\partial}{\partial x_i}\left[\left(\mu + \frac{\mu_t}{\sigma_k}\right)\frac{\partial k}{\partial x_i}\right] + G_k - \rho\varepsilon. \tag{5}$$

$$\frac{\partial}{\partial x_i}(\rho u_i \varepsilon) = \frac{\partial}{\partial x_i}\left[\left(\mu + \frac{\mu_t}{\sigma_\varepsilon}\right)\frac{\partial \varepsilon}{\partial x_i}\right] + C_{1\varepsilon}G_k\frac{\varepsilon}{k} - C_{2\varepsilon}\rho\frac{\varepsilon^2}{k}. \tag{6}$$

The term G_k is the generation of turbulence kinetic energy due to the mean velocity gradients. The turbulent viscosity, μ_t, is calculated from the equation

$$\mu_t = \rho C_\mu \frac{k^2}{\varepsilon} \tag{7}$$

and the effective heat conductivity (λ_{eff}) is calculated by

$$\lambda_{eff} = \lambda + \frac{c_p \mu_t}{Pr_t}. \tag{8}$$

The constants $C_{1\varepsilon}$, $C_{2\varepsilon}$, C_μ, σ_k, and σ_ε used are: $C_{1\varepsilon} = 1.44$, $C_{2\varepsilon} = 1.92$, $C_\mu = 0.09$, $\sigma_k = 1.0$, $\sigma_\varepsilon = 1.3$ [10]. The constant Pr_t is set to 0.85. The equations may include more other source terms, for example, turbulence kinetic energy due to buoyancy and the contribution of fluctuating dilatation in compressible turbulence. In general, the standard k-ε model should be used together with the near-wall treatment due to the wall effect on the turbulence. In this study the standard wall functions are selected. More details can be found from [11].

Boundary Conditions - Based on several real applications, uniform velocity of 10 m/s is assigned to the inlet of all the four domains, which is corresponding to a mass flow rate of about 46 kg/s. The temperature of inlet air is 90 ^oF. The inlet conditions of the turbulence are 1 m^2/s^2 for the turbulence kinetic energy and 1 m^2/s^3 for the dissipation rate, which is equivalent to a turbulent intensity of 1%. The flow exit (outlet) is assumed to have a constant pressure. The backflow (reverse flow), if any, is set to 90 ^oF. The sidewall is non-slip (velocity is zero at the wall) and is assumed to be adiabatic.

Humidity - It is known that relative humidity has a strong effect on fog cooling effectiveness: the higher the relative humidity, the lower the performance of the fog cooling is. Three levels of relative humidity are considered in this study: 0 (dry air), 30%, and 60%.

Discrete Phase (Water Droplets)

Droplet Flow and Heat Transfer - Basically, the droplets in the airflow can encounter inertia and hydrodynamic drags. They can also get heating or cooling from the continuous phase. After the droplet is evaporated due to either high temperature or low moisture partial pressure, the vapor diffuses into the main flow and is transported away. The rate of vaporization is governed by gradient diffusion and the corresponding mass change rate of the droplet can be given by,

$$\frac{dm_p}{dt} = \pi d^2 k_c (C_s - C_\infty) \tag{9}$$

where k_c is the mass transfer coefficient and C_s is the concentration of the vapor at the droplet surface, which is evaluated by assuming that the flow over the surface is saturated. C_∞ is the vapor concentration of the bulk flow, obtained by solving the transport equations. The value of k_c can be calculated from an empirical correlation for droplet evaporation [12, 13],

$$Sh_d = \frac{k_c d}{D} = 2.0 + 0.6 Re_d^{0.5} Sc^{0.33} \tag{10}$$

where Sh is the Sherwood number, Sc is the Schmidt number (defined as ν/D), and D is the diffusion coefficient of vapor in the bulk flow.

Because of the forces encountered by a droplet in a flow field, the droplet can be either accelerated or decelerated. The velocity change can be formulated by

$$d\mathbf{v_p}/dt = \mathbf{F_d} + \mathbf{F_g} + \mathbf{F_o} \quad (11)$$

where $\mathbf{F_d}$ is the drag of the fluid on the droplet and $\mathbf{F_g}$ is the gravity. $\mathbf{F_o}$ represents the other forces, and $\mathbf{v_p}$ is the droplet velocity (vector). Among the forces represented by F_o, typically they can include the "virtual mass" force, thermophoretic force, Brownian force, Saffman's lift force, etc.

The heat transfer between droplets and the continuous phase can cause the droplet temperature change. Without considering radiation heat transfer, its sensible heat change depends on the convective and latent heat transfer, as shown in the following equation.

$$m_p c_p \frac{dT}{dt} = \pi d^2 h(T_\infty - T) + \frac{dm_p}{dt} h_{fg} \quad (12)$$

where h_{fg} is the latent heat, and h is the convective heat transfer coefficient, which is calculated by the equation of heat/mass analogy from Eq. 10.

$$Nu_d = \frac{hd}{\lambda} = 2.0 + 0.6\,Re_d^{0.5}\,Pr^{0.33} \quad (13)$$

where Pr is the Prandtl number and λ the heat conductivity of the bulk flow.

Stochastic Particle Tracking - The effects of turbulence on the dispersion of particles can be considered by using stochastic tracking. Basically, the droplet trajectories are calculated by using the instantaneous flow velocity ($\bar{u} + u'$) rather than the average velocity ($\bar{u}$). The velocity fluctuations are then given as:

$$u' = \varsigma\left(\overline{u'^2}\right)^{0.5} = \varsigma(2k/3)^{0.5} \quad (14)$$

where ζ is a normally distributed random number. This velocity will apply during the characteristic lifetime of the eddy (t_e), a time scale defined by either of the following equations.

$$t_e = 0.3k/\varepsilon \quad (15)$$

$$t_e = -0.15k/\varepsilon \log(r) \quad (16)$$

where r is a uniform distributed random number ranging from 0 to 1. In case the droplet slip velocity is so large that the time for the droplet to cross the eddy is shorter than the time defined above, the droplet eddy crossing time will be used, which is defined as:

$$t_{cross} = -t_p \ln[1 - L_e/(t_p\,|\,u - u_p\,|)] \quad (17)$$

where t_p is the particle relaxation time with $t_p = \rho_p d_p^2/(18\rho_g \nu_g)$, L_e is the eddy length scale, and $|u-u_p|$ is the magnitude of the relative velocity. After this time period, the instantaneous velocity will be updated with a new ζ value until a full trajectory is obtained. The random effect of the turbulence on the droplets can predicted reasonably only if a sufficient number of trajectories are calculated. In this study the trajectory number is chosen to be 50 and it is found that increasing this number does not make the result much different.

There are other methods to model the droplet turbulence dispersion, and more details, together numerical implementation in Fluent, can be found from [11].

Mist Injection and Droplet Sizes - Different from experimental studies, the control of droplets can be easily implemented in a numerical simulation. The boundary condition of droplets at walls is assigned as "reflect", which means the droplets elastically rebound off the wall once reaching the wall. A more complex model is undertaken to determine if the droplets breakup, rebound, or are trapped by the wall when they hit the wall. At the outlet, the droplets just simply flee/escape from the computational domain.

Depending on the relative humidity, the amount of water injected hinges on the water required to reach 100% humidity. For example, air at 90 °F and 60% humidity has moisture of 1.78% (mass fraction). To reach 100% humidity (with a saturation temperature of 78 °F), the water injection is given to 0.0028 kg per kilogram of dry air. The water droplets are injected into the computational domain with the same velocity of the airflow. There are totally 16 locations uniformly distributed close to the inlet. The mass flow rate is the same at each injection location, i.e., 1/16th of the total droplet mass flow rate.

Since the evaporation rate is also strongly related to the droplet size, the effect of different droplet sizes on cooling performance are investigated in this study. The first step is to use uniform droplets of 5, 10 and 50 μm, respectively. The second step is to use a distributed size from the laboratory results of Li et al. [14] who used impact-pin nozzles (manufactured by MEE Industries) to generate mist. The nonuniform droplet size distribution is given in Fig. 2 and detailed values are provided in Table 1. The smallest droplets are 5 μm and the largest are 50 μm. This distribution gives an average diameter of d_{10}= 12.8μm, d_{20} = 14.6μm, d_{30}=16.7μm and d_{32} = 21.8μm. The Dv90 of this distribution is 40μm.

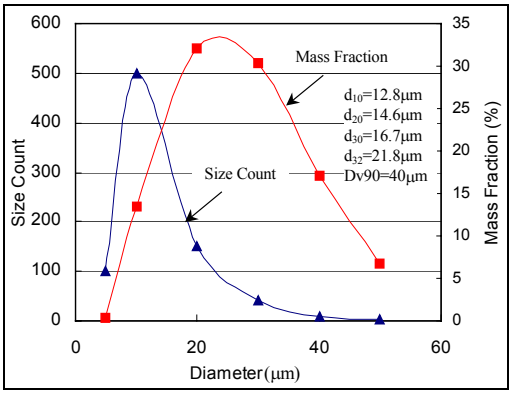

Figure 2 Distributed Droplet Sizes from Li et al. [14]

Table 1 Droplet Size Distribution

Diameter (μm)	5	10	20	30	40	50
Droplet count	100	500	150	42	10	2
Mass fraction (%)	0.33	13.38	32.12	30.35	17.13	6.69

Meshes and Convergence

Structured grids are used in this study and different meshes have been tested for grid dependence. Figure 3 shows the grid structure of one x-y plane. The grid number is 60~150 in the longitudinal (streamwise) direction and 15~25 in both the transverse y- and z-directions. A converged result can be reached after iteration proceeds alternatively between the continuous and discrete phases. Ten iterations in continuous phase are conducted between two iterations in the discrete phase. A typical converged result renders mass residues of 10^{-3}, energy residue of 10^{-6}, and momentum and turbulence kinetic energy residues of 10^{-4}. Typically, 600 to 1000

iterations are needed to obtain a converged result, which takes about 3 to 5 hours on a PC with Pentium 4 processor of 2.4 GHz.

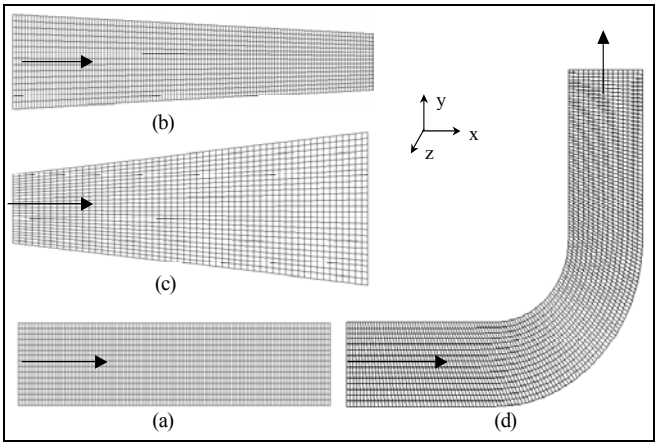

Figure 3 Mesh (a) Straight pipe 15x15x150 (b) Contraction 15x15x146 (c) Diffuser 25x25x60 (d) 90°-bend 15x15x150

Results and Discussion

The results of the straight pipe are shown in Figs 4-8. Figure 4 shows the temperature distribution in the straight pipe. The humidity in this case is 60%, and the droplet diameter (uniform) is 10 μm. It can be seen that water mist reduces the flow bulk temperature to about 78°F, consistent with the theoretical wet-bulb temperature. Figure 4 also shows that the overall temperature distribution is uniform, except near the inlet region. The distance to reach a uniform temperature distribution is less than 2 meters (or one hydrodynamic diameter of the duct) after injection. The uniform temperature is believed partially due to the turbulent mixing of the droplets with fluid and partially from the droplet diffusion. Note that the temperature close to the wall is high, almost all the way to the exit. The reason is that the injections are displaced away from the wall on purpose. In this way, the frequency of liquid deposit on the wall surface can be minimized. As shown in Fig. 5, adding additional injections close to the wall while keeping the total water mass flow rate constant brings down the wall temperature quickly. These near-wall injections do not seem to provide any more advantage for cooling the core air stream but consume more water to cool the wall. Therefore, it is advised that the near-wall injections be avoided in real application.

Further analysis shows that about 60% of the droplets are evaporated completely before exiting the duct, and the others will escape from the exit with reduced sizes (partial evaporation). Figure 6(a) shows the trajectories of some droplets, colored by the continuous change of droplet size. Note that the trajectories are not straight lines although the streamlines of the mainstream are straight. This is the result of stochastic turbulent dispersion effect, as mentioned earlier. Results of two stochastic tracking are shown for each injection at two different instances (Fig. 6a). Five of the traced trajectories show that the water droplets are completely evaporated. Disengaging the effect of stochastic turbulent dispersion results in straight trajectories parallel to the sidewalls (Fig. 6b). Considering both Figs. 4 and 6, we can conclude that the evaporation will only occur strongly at the beginning because of the high local temperature and low relative humidity. Downstream, the temperature decreases and the relative humidity increases, so the droplets evaporation rate degrades. Note that the average residence time of the droplets in the duct is about 0.8s (8m in length with a velocity of 10 m/s). Thus, the effective evaporation time is about 0.2 second.

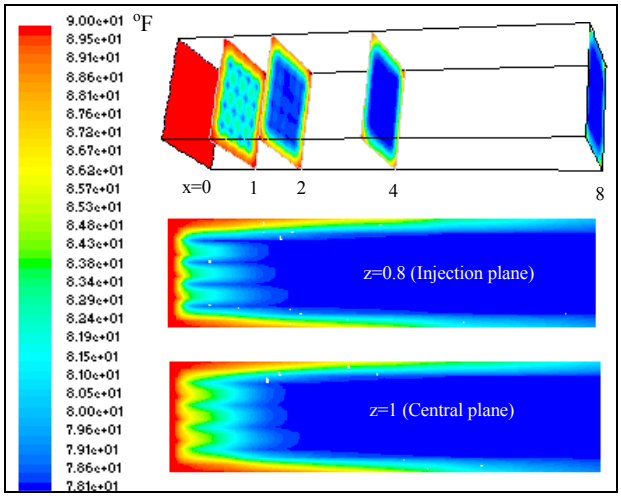

Figure 4 Temperature Distribution of Straight Pipe with 60% Relative Humidity and 10-μm Droplets

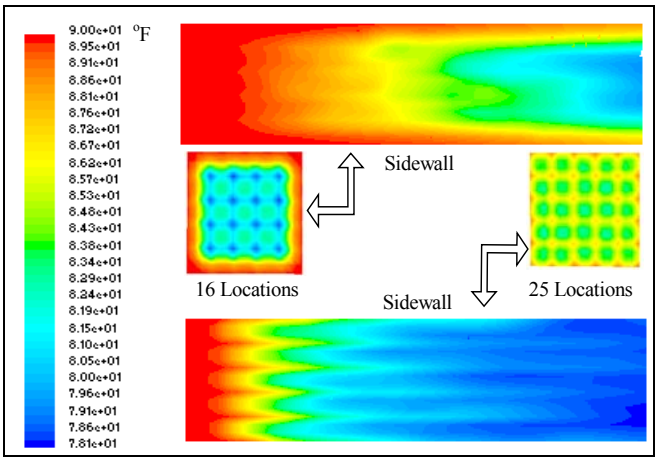

Figure 5 Effect of Near-Wall Injections on Wall Temperature

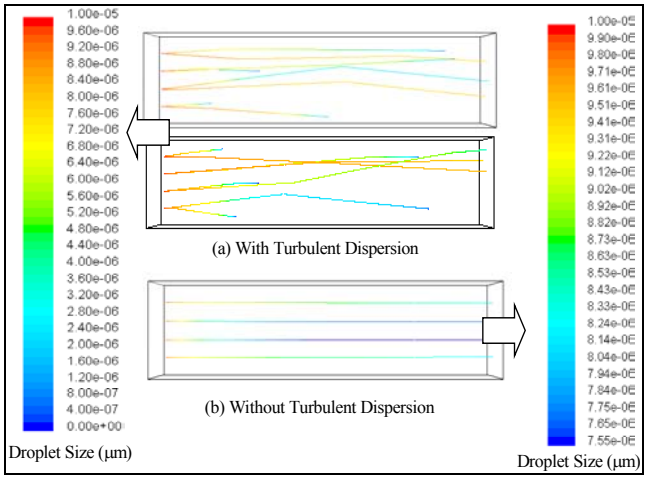

Figure 6 Droplet Trajectories in the Straight Pipe with 60% Relative Humidity and 10-μm Droplets

Effect of Relative Humidity

The effect of relative humidity is shown in Fig. 7, which clearly indicates that fog cooling becomes more effective when the humidity decreases. While the temperature at 30% humidity can reach 68 °F, the lowest temperature at 0% humidity (dry air) is 53 °F, both of which are consistent with the theoretical saturated temperatures. Except for detailed values of the local temperature distribution, it can be found that the overall distribution is similar: the temperature of the bulk flow reduces quickly before x=2; the wall temperature keeps high; and there is a cold core inside. The reason for the similar distribution is the evaporation ratio of the droplet at the same size is controlled by relative humidity. The relative humidity increases rapidly to 100% after droplet injections.

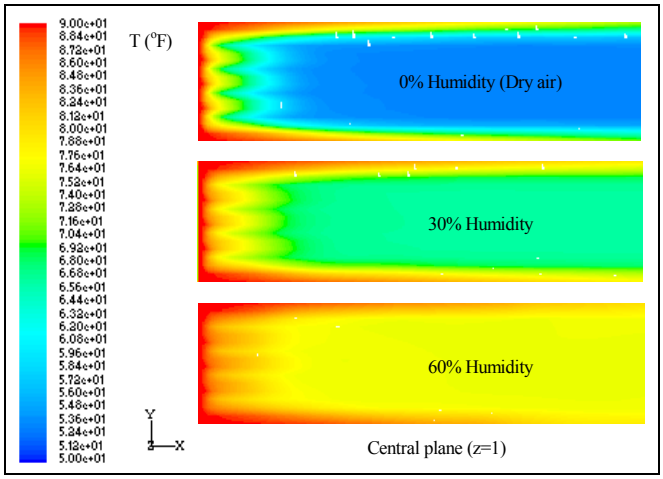

Figure 7 Temperature Distribution of Straight Pipe with Different Humidities (10-μm Droplets)

Effect of Droplet Size

Besides the relative humidity, droplet size can also affect the fog cooling. Figure 8 shows the temperature distribution with different droplet sizes but with the same relative humidity. The total mass fraction of the injection is also the same. Since smaller droplets make evaporation easier, the flow temperature reduces more quickly when smaller droplets are used. On the other hand, big droplets may not have enough time to complete evaporation before they arrive at the exit. This can lead to water droplets entering into the compressor stage, which may cause potential damages to the blades.

When the droplet size changes from 5 to 10 μm, the temperature distribution does not change much, and the lowest temperature is about the same because in both cases the relative humidity reaches 100%. However, when droplets of 50 μm are used, the temperature can only be reduced to 82°F and the highest relative humidity is about 85%. The duct is not long enough to evaporate all the big droplets in this case; so the air is not saturated and droplets escape from the exit with an average diameter of about 38 μm. In real applications, the average droplet size is below 10 μm, but a small percentage of droplets can be as large as 50 μm; therefore, the study of 50μm can help predict the residual size distribution of large particles at the exit of the duct. The information of particle size distribution is important for overspray and protecting compressor blades from excessive erosions.

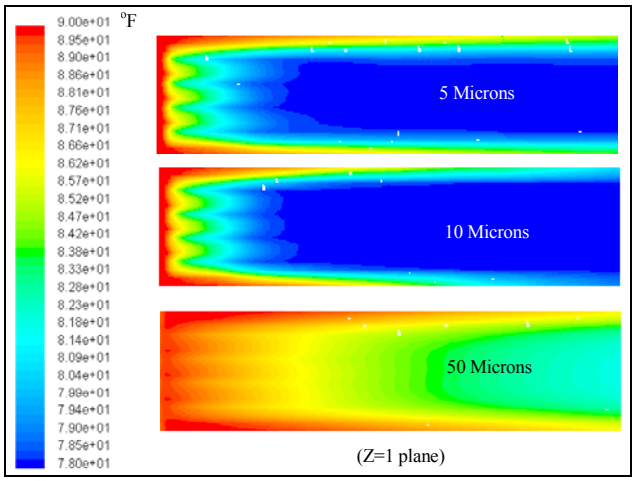

Figure 8 Temperature Distributions of Different Initial Droplet Sizes in the Straight Pipe with 60% Humidity

Effect of Droplet Size Distribution

In a real application, the injected droplet size is not a single value. After examining the behavior of uniform droplet size, investigation of the influence of nonuniform droplet size distribution follows. Figure 9 shows the temperature field using the distributed droplet sizes. The temperature field reflects the combined characteristics of different uniform droplet size presented earlier. First, the overall temperature reduces slowly (compared with Fig. 4) due to the presence of large droplets. Secondly, the temperature at the center area of the outlet reaches the saturated temperature faster than outside due to small droplets. The temperature distribution is not as uniform as that shown in Fig. 4. The trajectories show that more droplets survive at the exit of the duct than those shown in Fig. 6 with uniform 10-μm droplets. The overall temperature at the exit is 82 °F.

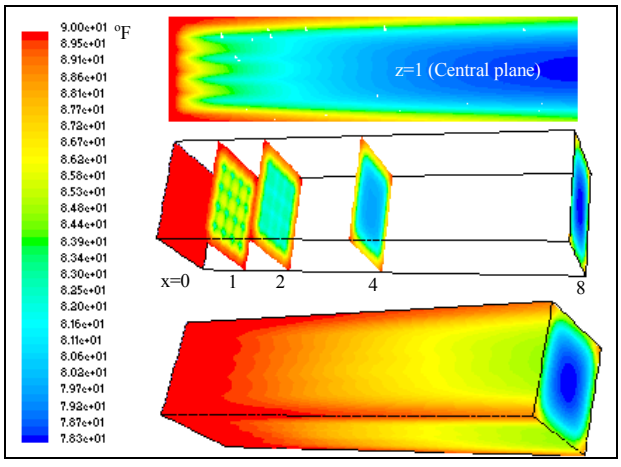

Figure 9 Temperature Distribution in the Straight Pipe with 60% Humidity and Distributed Droplet Sizes

To compare the results of different cases effectively, the distributions of averaged temperature are plotted in Fig. 10. Once again, the figure shows that a large temperature drop occurs within 2 meters and the effect of relative humidity is more pronounced than that of droplet size. To evaluate the performance of fog cooling, the cooling effectiveness is defined as

$$\eta = \frac{T_{amb} - T_{exit}}{T_{amb} - T_{WBT}} \qquad (18)$$

where T_{amb} is the ambient temperature or the inlet temperature of the cooling duct, T_{exit} is the average temperature at the exit, and T_{WBT} is the wet bulb temperature at the given humidity. The cooling effectiveness in different cases is summarized in Table 2. Also included in the table are T_{WBT}, T_{exit}, and the percentage of droplet evaporation in the duct. It can be seen that the percentage of droplet evaporation is very close to the cooling effectiveness, which is the result of energy conservation and the approach of using mass-weighted average temperature in calculating cooling effectiveness. Table 2 also shows that large droplets (50-μm) produce much lower effectiveness than small droplets (5- or 10-μm), while the cooling effectiveness slightly increases when relative humidity increases.

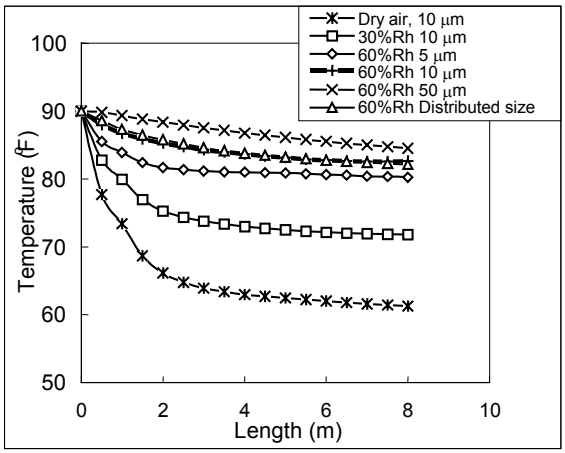

Figure 10 Average Temperature Distributions of Straight Pipe

Table 2 Fog Cooling in the Straight Pipe

Cases	T_{WBT} (°F)	T_{exit} (Average) (°F)	Droplet Evaporation (%)	η
Dry air, 10 μm	52.8	59.47	83.6	0.821
30% Rh, 10 μm	67.1	71.10	80.6	0.826
60% Rh, 5 μm	78.3	79.63	88.7	0.887
60% Rh, 10 μm	78.3	79.73	86.9	0.878
60% Rh, 50 μm	78.3	83.81	52.9	0.529
60% Rh, Distributed size	78.3	81.09	76.2	0.762

Effect of Duct Geometry

To investigate the influence of pressure gradients on particle dynamics, three simple, fundamental geometries are applied. The favorable pressure gradient (or acceleration effect) is studied in a contraction (or nozzle); the adverse pressure gradient effect (or deceleration effect) is in a diffuser; and the body force effect (or centrifugal force effect) is in a 90° bend. Temperature distributions are shown in Fig. 11. Compared to the straight duct under the same humidity and droplet size, the lowest temperature is about the same. A detailed examination shows that at the diffuser exit there exists a relatively large area surrounding the cold core without significant cooling. This could be due to the inertia effect as well as low diffusion rate of the droplets. The flow separates and reverse flow occurs at the exit (see Figs. 11 and 12), which also contributes to this effect. As shown in Fig. 12, the reverse flow occurs mainly in the corners. The temperature of the 90° bend shows lowest temperature migrating to the outer wall of the exit. The centrifugal force, together with the secondary flow, redistributes the mist concentration, which is no longer uniform. The area with more droplets near the outer wall results in lower temperatures.

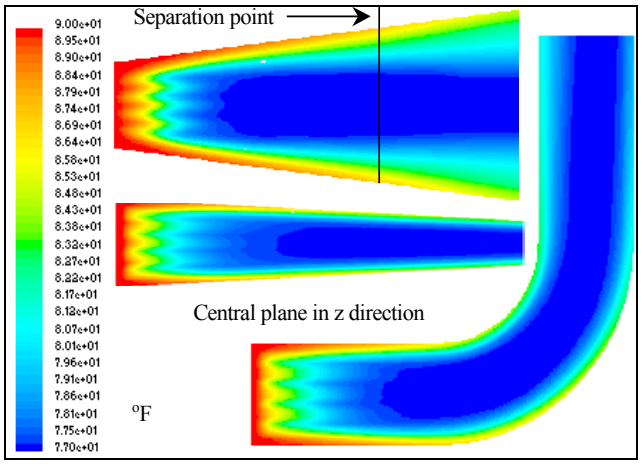

Figure 11 Temperature Fields in A Contraction, A Diffuser, and A 90° Bend with 60% Humidity and 10-μm Droplets

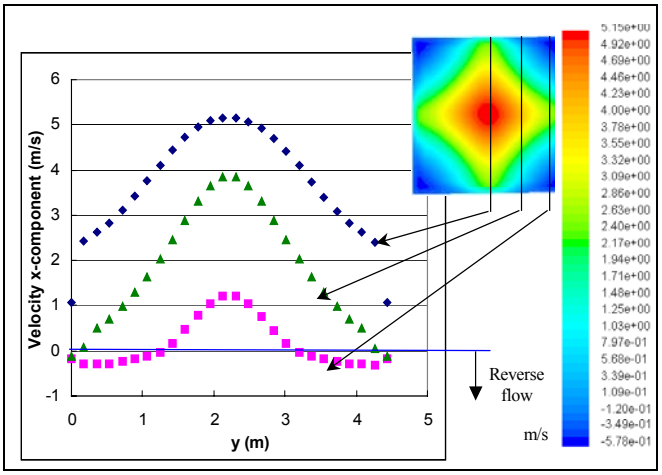

Figure 12 Outlet Velocity Profile of A Diffuser (Reverse Flow Occurs at Four Corners)

To further explore the effect of the centrifugal force and the induced secondary flow on larger droplet cooling in the 90° bend, results with 50-μm droplets are shown in Fig. 13. Compared to the result in Fig. 11, the larger droplets make the migration of lowest temperature more apparent. The droplet trajectory in this figure clearly shows more droplets moving outward in the 90° bend under the influence of centrifugal force. This trend results in the lowest temperature (81°F) occurring near the outer wall while the area close to the inner wall is around 83°F. This non-uniform cooling makes the average temperature at the exit a bit higher than other cases. Non-uniform temperature distribution at the inlet of the compressor is not preferred. Auxiliary device is needed to even out a non-uniform temperature distribution if the temperature variation becomes large. Same as in the straight pipe, the big droplets cannot complete the evaporation in the 90° bend. The average droplet size at the exit is 34 μm.

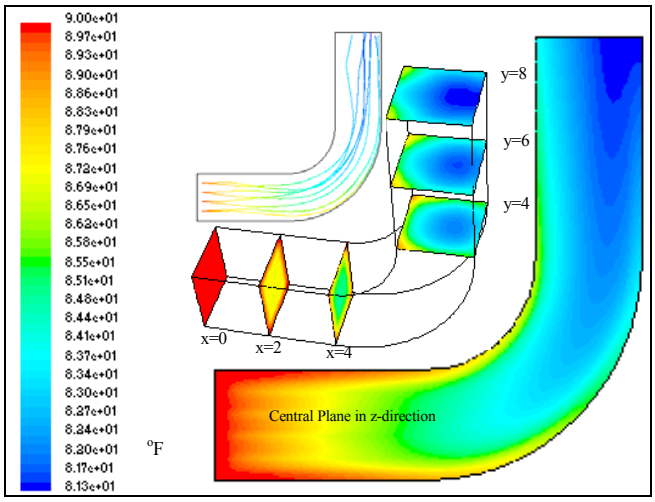

Figure 13 Temperature Distribution in the 90-degree Bend with 60% Humidity and 50-μm Droplets

Simulations are also conducted on the effects of humidity and droplet size on the fog cooling when different geometries are used. Results are summarized in Figures 14-16 and Tables 3-5. More detailed analysis is documented in Pinninti et al. [15]. These figures and tables show the similar trends to those presented in the straight pipe. Because of the reverse flow in the diffuser, the average temperature increases near the exit. Correspondingly, the cooling effectiveness reduces when compared to the droplet evaporation ratio (see Table 3). High evaporation ratio is due to the high average temperature as well as lower flow velocity near exit of the diffuser. Note that the droplet evaporation rate is the same as the cooling effectiveness for all other cases.

The effect of acceleration is shown in Fig. 15 and Table 4. The cooling effectiveness is slightly increased in the contraction for small droplets. However, acceleration in the contraction shortens the time for evaporation of large droplets (50 μm), which significantly lowers the cooling effectiveness to merely 33%.

The cooling effectiveness in the 90° bend is the highest among all cases except for larger droplets at 50 μm. This increased cooling is attributed to the secondary flow mixing and the relatively longer duct, which is about 3 meters longer than the contraction and diffuser.

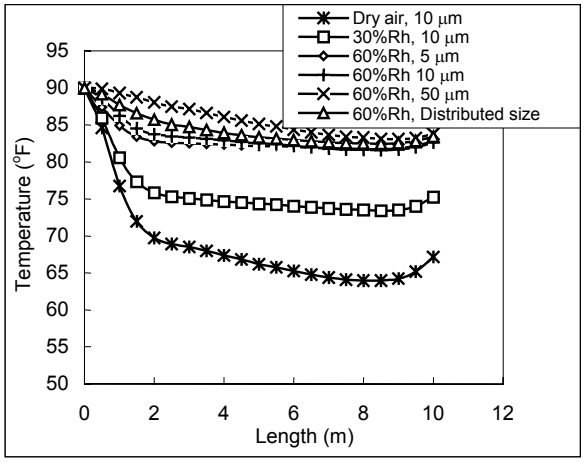

Figure 14 Average Temperature Distributions of Diffuser

Table 3 Fog Cooling in the Diffuser

Cases	T_{WBT} (°F)	T_{exit} (Average) (°F)	Droplet Evaporation (%)	η
Dry air, 10 μm	52.8	59.19	90.6	0.828
30% Rh, 10 μm	67.1	70.45	90.8	0.854
60% Rh, 5 μm	78.3	79.74	93.8	0.877
60% Rh, 10 μm	78.3	79.81	93.6	0.871
60% Rh, 50 μm	78.3	81.28	80.8	0.746
60% Rh, Distributed size	78.3	80.42	87.7	0.818

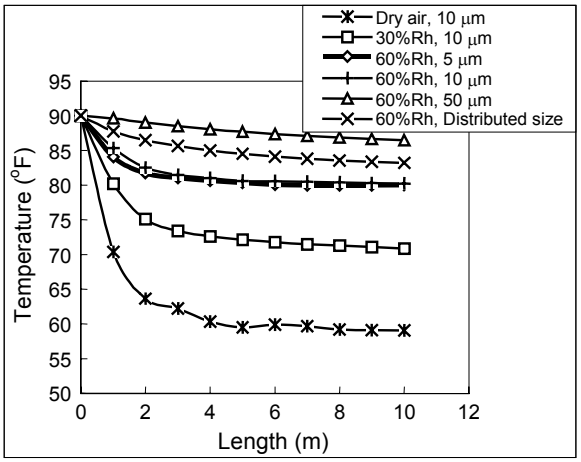

Figure 15 Average Temperature Distributions of Contraction

Table 4 Fog Cooling in the Contraction

Cases	T_{WBT} (°F)	T_{exit} (Average) (°F)	η or Droplet Evaporation Ratio
Dry air, 10 μm	52.8	58.47	0.847
30% Rh, 10 μm	67.1	70.06	0.871
60% Rh, 5 μm	78.3	79.24	0.920
60% Rh, 10 μm	78.3	79.54	0.894
60% Rh, 50 μm	78.3	86.09	0.334
60% Rh, Distributed size	78.3	82.49	0.642

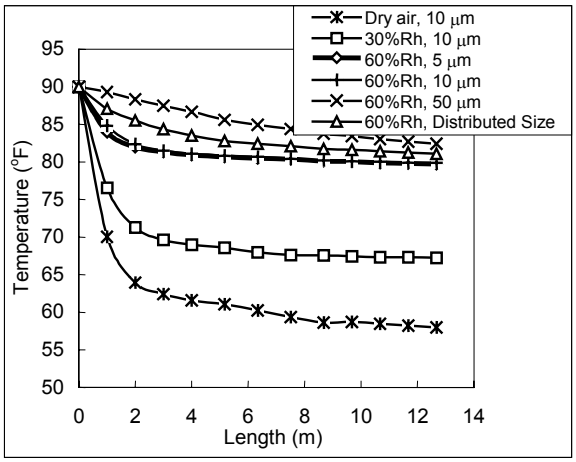

Figure 16 Average Temperature Distributions of 90° Bend

Table 5 Fog Cooling in the 90° Bend

Cases	T_{WBT} (°F)	T_{exit} (Average) (°F)	η or Droplet Evaporation Ratio
Dry air, 10 μm	52.8	56.72	0.895
30% Rh, 10 μm	67.1	68.77	0.927
60% Rh, 5 μm	78.3	78.88	0.950
60% Rh, 10 μm	78.3	78.90	0.948
60% Rh, 50 μm	78.3	82.42	0.648
60% Rh, Distributed size	78.3	80.06	0.850

Fog Cooling with a Complex Duct

In real applications, the passage ducts are often constructed to accommodate the existing turbine inlet structures. Hence, the geometry could be simple or complex. A complex duct similar to a real application is employed for analysis as shown in Fig. 17. The duct has an inlet of 2.1×3.5 m^2 and outlet of 2.1×1.2 m^2. The inlet velocity is set to 5 m/s. The inlet flow has a relative humidity of 60%, and the injection droplet size is 10 μm.

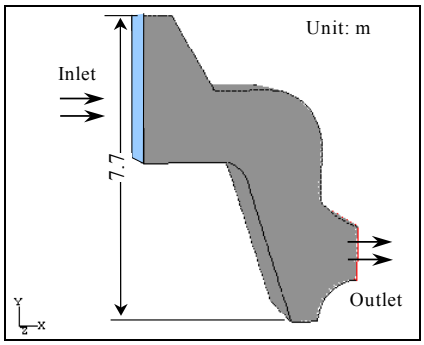

Figure 17 A Complex Cooling Duct in a Real Application

Numerical results of velocity and temperature field in the center plane along the z-direction are shown in Fig. 18. It can be seen that two large recirculation regions are visible in the duct. These recirculations should be removed or minimized because they present three disadvantages: (a) they produce flow pulsation and cause low-frequency pressure waves that travel with sonic speed to the downstream compressor and can affect compressor performance; (b) they induce aerodynamic losses by producing irreversible energy dissipation; and (c) they trap water droplets and allow water droplets to coalesce into bigger droplets or water filaments larger than 100μm, which can cause irrecoverable damages to compressor blades if they are entrained into the compressor. Since no coalesce model is employed in this study, this potential coalescence problem is not investigated but will be in the future. The lowest temperature is about 78 °F, which again is consistent with the saturation temperature of the inlet flow. Since most of the droplets follow the main air stream quite well, the cooling effect inside the main core stream is the most significant.

Figure 19 shows the droplet trajectories in the central plane of the duct, colored by residential time. Most of the droplets (up to 80%) evaporate, and the rest follow the main stream to the exit. The overall average temperature at the exit is 79.4 °F, which is higher than the saturation temperature. The injection arrangement can be further optimized to obtain uniform cooling performance at the exit.

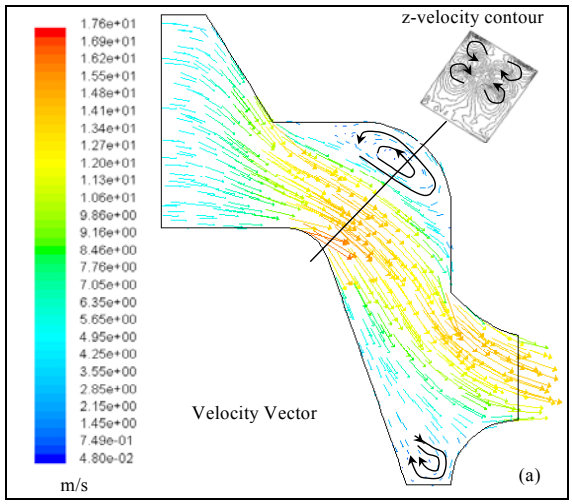

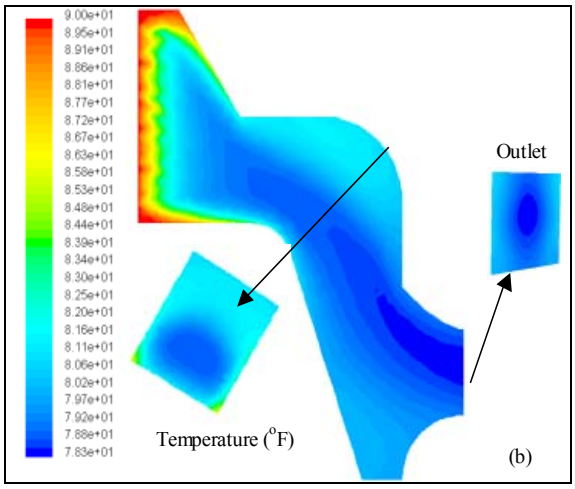

Figure 18 Velocity and Temperature Fields on the Central Plane in a Complex Duct with 10μm Water Droplets and 60% Relative Humidity (a) Velocity Field, (b) Temperature.

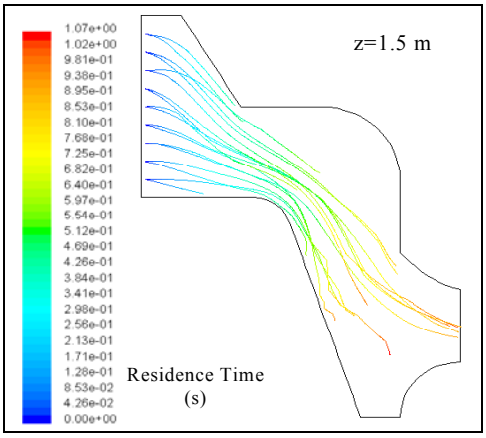

Figure 19 Droplet Trajectories in Complex Cooling Duct with 10μm Droplets and 60% Relative Humidity

Problems and future research

Collisions and coalescences of droplets are important phenomena in real applications especially at the beginning of the nozzle injection and near the entrance of the compressor. The small droplets can coalescence into larger ones and be carried into the compressor causing damage to the compressor blades. Another possibility is that big droplets do not follow the main air stream well, so they may collide with walls or other devices such as silencers and obstructions. The continuous deposits of water droplets on solid surfaces would result in liquid films that could be entrained and broken up as water filaments or large droplets and be carried into the compressor. The liquid films could also run down to the floor and accumulate into water puddles. Sheets of water entrained into the compressor are dangerous. Future work will model water droplet collisions and coalescence to predict liquid films forming on the wall and floor.

Conclusions

To investigate the mist transport in entrance ducts of various geometries, numerical simulations are performed in this paper. Fundamental geometries first considered include a straight duct, a diffuser, a contraction, and a 90-degree bend. Then, a complex duct representing a real application is employed for analysis. The effect of droplet size, droplet distribution, and humidity on fog cooling performance is examined. The conclusions are:

- Numerical simulation provides a detailed local temperature distribution resulted from fog-cooling process in a duct.
- Evaporation occurs mostly within 2 m after injection (0.2 second of the residence time) for those droplets less than 10 microns.
- In the contraction, the acceleration significantly lowers the cooling effectiveness when large droplets of 50-μm are used. However, the cooling effectiveness is slightly increased for small droplets.
- In the diffuser, the average temperature increases near the exit because of the reverse flow. Correspondingly, it shows a droplet evaporation ratio higher than the cooling effectiveness. High evaporation ratio is due to the high average temperature as well as lower flow velocity (for longer residence time) near exit of the diffuser.
- In the 90-degree bend, centrifugal force and secondary flow move the droplets toward the outer wall and result in a non-uniform temperature distribution at the exit with cooler area near the outer wall. High cooling effectiveness is achieved due to the secondary flow mixing and the relatively longer duct when compared with other cases.
- Simulation with a complex duct similar to those used in real applications shows regions of large recirculation. The recirculation regions should be removed or minimized because they produce flow pulsation, induce aerodynamic losses, and trap water droplets and allow water droplets to coalesce into larger ones that may be detrimental to the compressor blades.

Acknowledgement

This study is partially supported by the Louisiana Governor's Energy Initiative via the Clean Energy and Power Research Consortium (CPERC).

References

[1] Cortes, C. R. and Willems, D. E., 2003, "Gas Turbine Inlet Air Cooling Techniques: An Overview of Current Technologies," POWER-GEN International, Las Vegas, Neva, USA

[2] Chaker, M., Meher-Homji, C.B., Mee, M., 2002, "Inlet Fogging of Gas Turbine Engines - Part A: Fog Droplet Thermodynamics, Heat Transfer and Practical Considerations," ASME Proceedings of Turbo Expo 2002, Vol. 4, pp. 413-428.

[3] Bhargava, R. and Meher-Homji, C.B., 2002, "Parametric Analysis of Existing Gas Turbines with Inlet Evaporative and Overspray Fogging," ASME Proc. of Turbo Expo 2002, Vol. 4, pp. 387-401.

[4] Chaker, M., Meher-Homji, C.B., Mee, M., 2002, "Inlet Fogging of Gas Turbine Engines - Part B: Fog Droplet Sizing Aanalysis, Nozzle Types, Measurement and Testing," ASME Proceedings of Turbo Expo 2002, Vol. 4, pp. 429-441.

[5] Chaker, M., Meher-Homji, C.B., Mee, M., 2002, "Inlet Fogging of Gas Turbine Engines - Part C: Fog Behavior in Inlet Ducts, CFD Analysis and Wind Tunnel Experiments," ASME Proceedings of Turbo Expo 2002, Vol. 4, pp. 443-455.

[6] Gajjar, H., Chaker, M. et al., 2003, "Inlet fogging for a 655 MW combined cycle power plant- design, implementation and operating experience," ASME Proceedings of Turbo Expo 2003, Vol. 2, pp. 853-861.

[7] Willems, D. E. and Ritland, P.D., 2003, "A Pragmatic Approach to Evaluation of Inlet Fogging System Effectiveness," Proc. of Int. Joint Power Generation Conference, Paper No. IJPGC 2003-40075.

[8] Mahapatha, S. and Gilstrap, J.K., 2003, "Gas Turbine Inlet Air Cooling: Determination of Parameters to Evaluate Fogging Nozzle's Atomizing Performance," Proceedings of Int. Joint Power Generation Conference, Paper No. IJPGC 2003-40124.

[9] Mahapatha, S. and Gilstrap, J.K., 2003, "Gas Turbine Inlet Air Fogging Systems: Application of Psychometric Principles to Study Cooling and Humidification Process," Proc. of Int. Joint Power Generation Conference, Paper No. IJPGC 2003-40130.

[10] B. E. Launder and D. B. Spalding, 1972, *Lectures in Mathematical Models of Turbulence*, Academic Press, London, England.

[11] Fluent Manual, Version 6.1.22, 2003, Fluent, Inc.

[12] Ranz, W. E. and Marshall, W. R. Jr., 1952, "Evaporation from Drops, Part I," Chem. Eng. Prog., **48**, pp. 141-146.

[13] Ranz, W. E. and Marshall, W. R. Jr., 1952, "Evaporation from Drops, Part II," Chem. Eng. Prog., **48**, pp. 173-180.

[14] Li, X., Gaddis, J. L., Wang, T., 2001, "Modeling of Heat Transfer in a Mist/Steam Impinging Jet," ASME J. of Heat Transfer, **123**, pp. 1086-1092.

[15] Pinninti, V., Wang, T., and Li, X., 2004, "Simulation of Mist Transport for Gas Turbine Inlet Air Cooling," Report of the Energy Conversion and Conservation Center, ECCC 2004-05, University of New Orleans.